

Pressure-induced Zero Gap Semiconducting State in the Organic Conductor α -(BEDT-TTF) $_2$ I $_3$ Salt

Shinya Katayama, Akito Kobayashi and Yoshikazu Suzumura

Department of Physics, Nagoya University, Nagoya 464-8602

(Received February 8, 2020)

We show a zero gap semiconducting (ZGS) state in quasi-two-dimensional organic conductor α -(BEDT-TTF) $_2$ I $_3$ salt, which emerges under the uniaxial pressure along a-axis (the stacking axis of the BEDT-TTF molecule). The ZGS state is the state where a Dirac-cone with a band spectrum of the linear dispersion exists around the Fermi point connecting the unoccupied (electron) band and the occupied (hole) band. The angular dependence of the cone is anisotropic and also exhibits the difference in the velocity between the electron band and the hole band. By varying the magnitude of several transfer energies of the tight-binding model with four-sites in the unit cell, it is shown that the ZGS state exists in the wide region of the pressures, and is attributable to the large anisotropy of the transfer energies along the stacking axis.

KEYWORDS: zero gap semiconductor, α -(BEDT-TTF) $_2$ I $_3$, Dirac-cone, quarter-filling, organic conductor, BEDT-TTF, contact point

1. Introduction

Quasi-two-dimensional organic conductors, BEDT-TTF (bis(ethylene dithiolo)tetrathiofulvalene), exhibit several electronic states, such as Mott insulator, charge ordering and superconductivity,^{1,2} under the variation of temperature, hydrostatic pressure or uniaxial strain. The electronic states of these BEDT-TTF (ET) salts originate in the band structure of π -electrons with the several transfer integrals and the strong Coulomb interaction acting on-site and nearest neighbor sites. Among these ET salts, the unusual phenomena have been observed in the α -(ET) $_2$ I $_3$ (α phase of BEDT-TTF triiodide) salt,³ which consists of four molecules per unit cell with 3/4-filled band (i.e., quarter filled band of the hole). Under ambient pressure (A.P.), the α -(ET) $_2$ I $_3$ salt exhibits the metal-insulator transition at $T_{MI} = 135$ K and is followed by the charge ordering,⁴⁻⁹ which aligns along the b-direction perpendicular to the stacking axis (a-axis). When the uniaxial strain with 2kbar is applied along a-direction, the salt undergoes superconducting state at 7K.^{10,11} Under high pressures, the α -(ET) $_2$ I $_3$ salt exhibits an exotic property which is associated with narrow gap semiconducting (NGS) state.^{5,6} At 20 kbar of hydrostatic pressure, the resistivity becomes rather metallic and is almost independent of temperature between 300K and 1.5K, although the carrier density, n , decreases from 10^{21}cm^{-3} (300K) to 10^{15}cm^{-3} (1K). It has been claimed that such a temperature dependence may be originated from the NGS state with a gap $E_g \sim 1\text{meV}$.⁶ There exists a difference in the effect of the uniaxial pressure between the a -direction (P_a) and the b -direction (P_b).¹¹ For a compression along the a -direction, the pressure-dependence of T_{MI} is small and the NGS state emerges for $P_a > 5$. For the uniaxial strain along the b-direction, the metal-insulator transition is suppressed noticeably while no superconducting transition and no NGS state occur at low temperatures.

The ordered state in α -(ET) $_2$ I $_3$ has been investigated theoretically, where the charge ordering state with the

horizontal pattern was obtained by using Hartree-Fock approximation^{12,13} and the superconducting state in the presence of the charge ordering was clarified in terms of the random phase approximation.^{14,15} It is noted that such a superconducting state occurs just before the onset of the NGS state under a-axis pressure. However the origin of the NGS state is not yet clear although the uniaxial pressure along a-axis favors the NGS state in α -(ET) $_2$ I $_3$.

In the present paper, we examine the pressure dependence of the band structure of the α -(ET) $_2$ I $_3$ salt within the tight-binding model in order to understand the NGS state, which emerges and is retained in the wide range of uniaxial pressure along a-axis. In §2, the extrapolation formula for the pressure dependence on transfer energies of the α -(ET) $_2$ I $_3$ salt is given where we employ the experimental data obtained from the X-ray diffraction experiment under pressures along both a-axis and b-axis.^{16,17} In §3, it is shown that the present organic conductor under the high pressure exhibits a zero gap semiconducting (ZGS) state with the Dirac-cone-like linear dispersion instead of the NGS state. Such a ZGS state under pressure is analyzed by varying transfer energies in §4. We also investigate the ZGS state in a more simplified model with two sites in the unit cell, in §5. Section 6 is devoted to discussion.

2. Formulation

In order to describe conduction electrons for the ET salts, we start with a two dimensional lattice model, which consists of four sites of ET molecules in the unit cell as shown in Fig. 1. The Hamiltonian is given by

$$H = \sum_{\langle i\alpha; j\beta \rangle} t_{i\alpha; j\beta} c_{i\alpha}^\dagger c_{j\beta}, \quad (1)$$

where $t_{i\alpha; j\beta}$ is the transfer energy from (i, α) site to the nearest neighbor (j, β) site. In eq. (1), $i, j (= 1, \dots, N_L)$ denote indices for the unit cell of the square lattice and $\alpha, \beta (= 1, 2, 3, 4)$ denote the indices in a unit cell. The

quantity $c_{i\alpha}$ is the annihilation operator of the conduction electron at (i, α) site. Using the Fourier transfor-

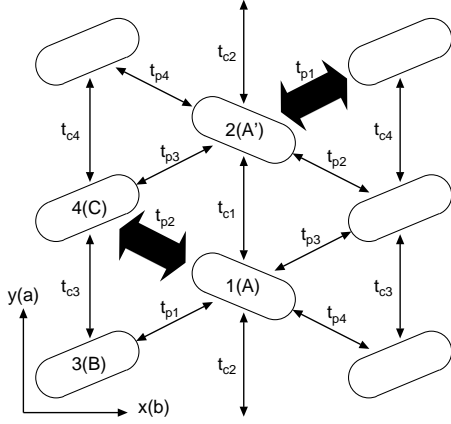


Fig. 1. Conducting plane of α -(ET) $_2$ I $_3$, where there are four ET molecules in the unit cell and the bond represents eight transfer energies ($t_{p1}, \dots, t_{p4}, t_{c1}, \dots, t_{c4}$). The $x(y)$ -axis corresponds to $b(a)$ -axis in Ref. 16. Thick arrows denote the dimerization in a model, which is considered in §5.

mation, $c_{\mathbf{k}\alpha} = N_L^{-1/2} \sum_{\mathbf{r}_i} \mathbf{k} e^{i\mathbf{k}\cdot\mathbf{r}_i} c_{i\alpha}$, eq. (1) is rewritten as

$$H = \sum_{\mathbf{k}, \alpha, \beta} \varepsilon_{\alpha\beta}(\mathbf{k}) c_{i\alpha}^\dagger c_{j\beta}, \quad (2)$$

where

$$\varepsilon_{\alpha\beta}(\mathbf{k}) = \frac{1}{N_L} t_{i\alpha:j\beta} \sum_{i,j} e^{i\mathbf{k}\cdot(\mathbf{r}_i - \mathbf{r}_j)}, \quad (3)$$

and $t_{i\alpha:j\beta}$ consist of eight transfer energies given by $t_{p1}, \dots, t_{p4}, t_{c1}, \dots, t_{c4}$ as shown in Fig. 1. In eq.(2), $\varepsilon_{\alpha\beta}(\mathbf{k})$ is expressed as

$$\begin{pmatrix} \varepsilon_{11}(\mathbf{k}) & \cdots & \varepsilon_{14}(\mathbf{k}) \\ \vdots & \ddots & \vdots \\ \varepsilon_{41}(\mathbf{k}) & \cdots & \varepsilon_{44}(\mathbf{k}) \end{pmatrix},$$

$$\begin{aligned} \varepsilon_{\alpha\alpha}(\mathbf{k}) &= 0 \quad (\alpha = 1, \dots, 4), \\ \varepsilon_{12}(\mathbf{k}) &= t_{c1} + t_{c2} e^{-ik_y}, \\ \varepsilon_{13}(\mathbf{k}) &= t_{p1} - t_{p4} e^{ik_x}, \\ \varepsilon_{14}(\mathbf{k}) &= t_{p2} - t_{p3} e^{ik_x}, \\ \varepsilon_{23}(\mathbf{k}) &= t_{p4} e^{ik_y} - t_{p1} e^{i(k_x + k_y)}, \\ \varepsilon_{24}(\mathbf{k}) &= t_{p3} - t_{p2} e^{ik_x}, \\ \varepsilon_{34}(\mathbf{k}) &= t_{c3} + t_{c4} e^{-ik_y}, \\ \varepsilon_{\alpha\beta}(\mathbf{k}) &= (\varepsilon_{\beta\alpha}(\mathbf{k}))^* \quad (\alpha \neq \beta), \end{aligned} \quad (4)$$

where k_x is replaced by $k_x + \pi$, and the suffix $x(y)$ corresponds to the $b(a)$ -axis.¹⁶ We determine the chemical potential by the 3/4 filling.

For the pressure dependence of transfer energies $t_{i\alpha:j\beta} = t_A, t'_A$, ($A = c1, c2, \dots, p4$) of α -(ET) $_2$ I $_3$, we

employ an extrapolation formula given by¹⁴

$$t_A(P) \simeq t_A(1 + K_A P), \quad (5)$$

$$t'_A(P) \simeq t_A(1 + K'_A P), \quad (6)$$

where P (kbar) denotes the pressure, and $t_A(P)$ ($t'_A(P)$) expresses the transfer energy under the pressure along a -axis (b -axis). By using the data of α -(ET) $_2$ I $_3$ salt for ambient pressure ($P=0$)¹⁶ and those for $P_a = 2$ and $P_b = 3$ at room temperature,¹⁷ the above coefficients are estimated as $t_{p1}, t_{p2}, t_{p3}, t_{p4}, t_{c1}, t_{c2}, t_{c3}, t_{c4} = 0.140, 0.123, -0.025, -0.062, 0.048, -0.020, -0.028, -0.028$, at ambient pressure and $K_{p1}, K_{p2}, K_{p3}, K_{p4}, K_{c1}, K_{c2}, K_{c3}, K_{c4} = 0.011, 0, 0, 0.032, 0.167, -0.025, 0.089, 0.089$ (0.024, 0.031, 0.053, 0.022, 0.042, 0.133, 0.167, 0.167) for pressures along a -axis (b -axis). As seen from K_A corresponding to the pressure along a -axis P_a , the large K_{c1} suggests that the pressure dependence is mainly determined by t_{c1} .

3. ZGS state

In this section, we focus on the electronic state under the pressure along a -axis, i.e., P_a . Since there are four sites in the unit cell, there are four energy bands, i.e., first, second, third and fourth bands from the top where the first band is almost empty and the rest is almost filled due to 3/4-filling. While, at ambient pressure, there is a small electron pocket close to $X(\pm\pi, 0)$ point and a hole pocket close to $Y(0, \pm\pi)$ point,⁶ these pockets are reduced for $P_a = 2$ kbar¹⁷ and reduced to a point for the wide range of further pressures along a -axis.^{14, 15} Actually from eq. (5), it is found that such an unusual state is retained for $P_a > 3$.

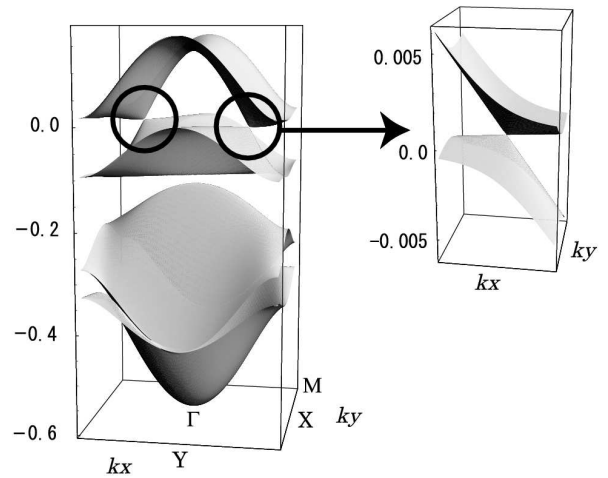


Fig. 2. Band dispersion of α -(ET) $_2$ I $_3$ at $P_a = 4$ kbar in the first Brillouin zone (left panel) and the enlarged one around the contact point at $\mathbf{k}^0 = (2.06, -0.91)$ (right panel) where the Fermi energy is taken as the origin.

Figure 2 shows the energy band spectrum of α -(ET) $_2$ I $_3$ at $p_a = 4$ kbar (left panel) on the plane of k_x

and k_y , which are scaled by the inverse of the lattice constant. The band consists of four bands where the first (electron) band is unoccupied while the second (hole) band is occupied. It should be noted that the contact point, i.e. the Fermi point, exists at $\pm \mathbf{k}^0$ in the circle. Actually, from eq. (4), the matrix element corresponding to the contact point, $\mathbf{k}^0 \simeq (2.06, -0.91)$, is obtained as $\varepsilon_{12} = 0.116 + 0.009i$, $\varepsilon_{13} = 0.150 - 0.082i$, $\varepsilon_{14} = 0.122 - 0.025i$, $\varepsilon_{23} = -0.152 + 0.079i$, $\varepsilon_{24} = -0.018 + 0.123i$, $\varepsilon_{34} = -0.095 + 0.032i$ which leads to four band energies, 0, 0, -0.184, -0.582, on the basis of the Fermi energy with $\varepsilon_F = 0.191$. The first band and the second band touch at the contact point, i.e., the hole and electron band degenerate on the point. Since the point has no relation to the symmetry, such a degeneracy occurs accidentally as first pointed out by Herring.¹⁸

It should be noted that the enlarged figure (right panel of Fig. 2) indicates a linear dispersion around the contact point at \mathbf{k}^0 . Such a state always exists for $P_a > 3$. The dispersion close to the contact point can be expressed as

$$E(\delta \mathbf{k})^\pm = v^\pm(\delta \mathbf{k})|\mathbf{k} - \mathbf{k}^0| \quad (7)$$

where $\delta \mathbf{k} = \mathbf{k} - \mathbf{k}^0$ and $v^+(\delta \mathbf{k})$ ($v^-(\delta \mathbf{k})$) is the velocity for the electron (hole) around the contact point. We call such a state as the Dirac cone according to the literatures.²¹⁻²⁴ In Fig. 3, the velocity $v^\pm(\delta \mathbf{k})$ around the contact point is shown as the function of θ , which is the angle between the vector $\delta \mathbf{k}$ and the k_x -axis. A noticeable angular variation in the velocity is seen with the relation:

$$v^+(\delta \mathbf{k}) \neq -v^-(\delta \mathbf{k}), \quad (8)$$

$$v^+(\delta \mathbf{k}) = -v^-(-\delta \mathbf{k}), \quad (9)$$

within the numerical accuracy of the present calculation.

The contact point for both cases of low pressure and high pressure is shown schematically as the function of the wave number in Fig. 4 where the contact point is seen at the bottom of the electron band. At low pressures of $P_a (\lesssim 3 \text{ kbar})$, one finds the metallic state where two contact points at \mathbf{k}^0 and $-\mathbf{k}^0$ exist below the Fermi energy ε_F . However, at high pressures of $P_a (\gtrsim 3 \text{ kbar})$, the contact point moves just on the Fermi energy, i.e., the emergence of the ZGS, which is retained due to the 3/4-filling. The property of ZGS state appears in the density of states $D(\omega)$ close to the Fermi energy, which is given by¹⁴

$$D(\omega) \propto |\omega|, \quad (10)$$

where $\omega = 0$ corresponds to the Fermi energy. Since $D(\omega)$ vanishes at the Fermi energy $\omega = 0$ i.e., leading to the zero gap, we call the state as the ZGS instead of the NGS.^{6,14} When the contact point is situated below the Fermi surface at low pressures, the corresponding cusp in the density of states is reduced and becomes negligibly small at ambient pressure.

In Fig. 5, the pressure dependence of the point contact, \mathbf{k}^0 is examined where the Fermi surface is shown for ambient pressure and $P_a = 2 \text{ kbar}$. With increasing pressure, the area of the Fermi surface is reduced as

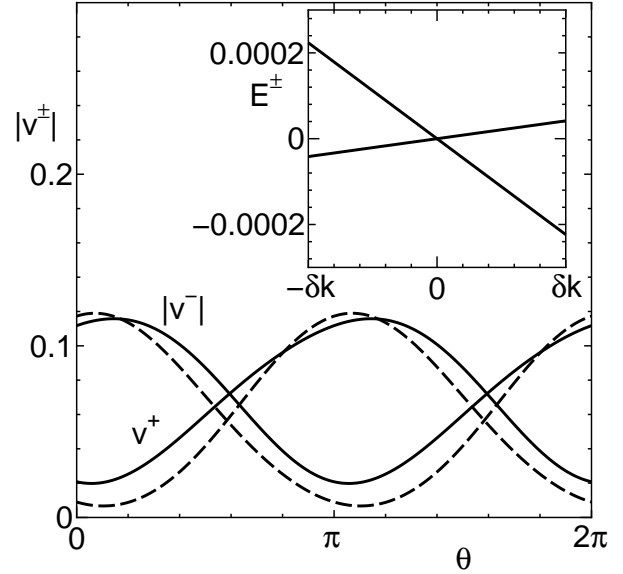


Fig. 3. Angular dependence of the velocity around the contact point (Dirac cone) at $P_a = 10 \text{ kbar}$ (solid line) and 5 kbar (dashed line) where θ (horizontal axis) denotes the angle between $\delta \mathbf{k}$ ($= \mathbf{k} - \mathbf{k}^0$) and the k_x -axis. The inset shows $E(\delta \mathbf{k})^\pm$ at $P_a = 10 \text{ kbar}$ where $\delta k > 0$ and < 0 correspond to $\theta = 0$ and π , respectively.

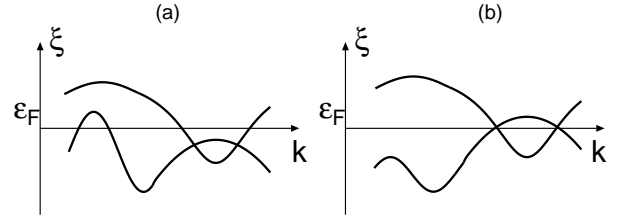


Fig. 4. Schematic band dispersion of the metallic state at low pressure (a) and that of the ZGS state at high pressure (b) where the wave number k (horizontal axis), is chosen so as to include the contact point.

seen from the electron (hole) pocket around the X (Y) point.¹⁷ The symbols represent the location of contact points at $P_a = 0, 2$ and 3 kbar , respectively. The arrow, which denotes the trajectory of \mathbf{k}^0 from $P_a = 0 \text{ kbar}$ to $P_a = 10 \text{ kbar}$, moves to the direction of the Γ point with increasing P_a . Here we note the temperature dependence of Fermi surface and the location of the point contact, \mathbf{k}^0 , in terms of the transfer energy at $P_a = 2 \text{ kbar}$ and $P_b = 3 \text{ kbar}$.¹⁷ With decreasing temperature, the change of the Fermi surface and \mathbf{k}^0 is small for $P_a = 2 \text{ kbar}$ while the Fermi surface is reduced appreciably and \mathbf{k}^0 moves so as to increase $|k_y^0|$ for $P_b = 3 \text{ kbar}$.

4. Stability of the contact point

In order to examine the stability of the contact point, we calculate the energy band spectra by varying magnitudes of the transfer energy from those of α -(ET)₂I₃. Since the difference between t_{c1} and t_{c2} is large for α -(ET)₂I₃, we employ a model, in which $t_{c1} \neq t_{c2}$ and the remained parameters are chosen as

$$t_{p1} = t_{p2} = 1, \quad t_{p3} = t_{p4}, \quad t_{c3} = t_{c4}. \quad (11)$$

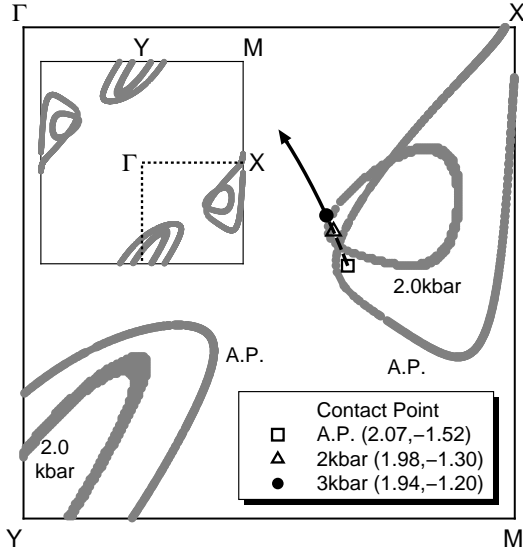


Fig. 5. Fermi surface (FS) of α -(ET) $_2$ I $_3$ at ambient pressure and $P_a = 2$ kbar where the main (inset) figure corresponds to a quarter (full) part of the first Brillouin zone. The arrow denotes the pressure dependence of the contact point which exists below the FS for $P_a < 3$ and just on the FS for $P_a > 3$. Symbols, square, triangle and circle which represent \mathbf{k}^0 for $P_a = 0, 2$ and 3 kbar, respectively.

Thus we examine a simplified model with independent energies, t_{c1} , t_{c2} , t_{p3} and t_{c3} .

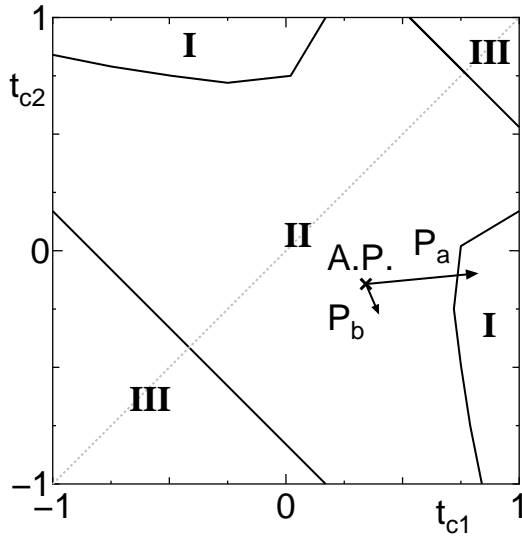


Fig. 6. Phase diagram on the plane of t_{c1} and t_{c2} for $t_{p3} = t_{p4} = t_{c3} = t_{c4} = -0.25$. The arrow denotes the pressure dependence of \mathbf{k}^0 for $0 < P_a < 10$ and $0 < P_b < 5$, respectively where the cross corresponds to the ambient pressure and transfer energies t_{c1} and t_{c2} are estimated from Eq. (5).

Figure 6 depicts a phase diagram on the plane of t_{c1} and t_{c2} for fixed $t_{p3} (= t_{p4} = t_{c3} = t_{c4}) = -0.25$. In Fig. 6, contact points exist in the regions of I and II, which corresponds to Fig. 5 (b) and (a), respectively. The region I denotes the ZGS state where the contact point becomes

equal to the Fermi point. The region II shows the semi-metallic state with the contact point being located below the Fermi energy. In the region III, the contact point disappears and the conventional metallic state is found. For Fig. 6, the contact point is obtained in the region enclosed by two lines

$$t_{c1} + t_{c2} = r_1, \quad t_{c1} + t_{c2} = r_2, \quad (12)$$

where $r_1 = 1.53$ and $r_2 = -0.83$. The boundary with the straight line originates from the choice of the parameter given by $t_{p3} = t_{p4} = t_{c3} = t_{c4}$. When parameters t_{c1} and t_{c2} take the value on the boundary of r_1 and r_2 i.e., between the region II and the region III, the contact point is given by the $\Gamma(X)$ point on the k_x - k_y plane in Fig. 6. The region I is obtained for large t_{c1} and $t_{c2} < 0$ (or large t_{c2} and $t_{c1} < 0$). Note that, the case of $t_{c1} = t_{c2}$ gives the metallic state with a special situation that the first band has the same energy as the second band on the line $k_y = \pm\pi$ in the first Brillouin zone. The van Hove singularity in the density of states exists near the Fermi energy when the parameters in region I are close to region II. When $|t_{p3}| (= |t_{p4}|)$ and $|t_{c3}| (= |t_{c4}|)$ are decreased, region II is reduced.

Here we comment on the pressure dependence of the contact point under the uniaxial pressure, P_a and P_b . As shown by the arrow in Fig. 6, the increase of P_a leads to the ZGS state but that of P_b is away from the NGS state since the increase of t_{c1} is large for P_a but is small for P_b .

5. Simplified model for the ZGS state

The ZGS state with contact points depends on the parameters of the transfer energy but some of them are redundant for the contact point. In §3, contact points are obtained for a model given by Fig. 1, which consists of four sites in the unit cell. In order to understand intuitively the NGS state, we examine the contact points by reducing further the parameter of the model into that with two sites in the unit cell.¹⁹

First, we ignore four transfer energies, $t_{p3}, t_{p4}, t_{c3}, t_{c4}$ in Fig. 1, since the NGS state with contact points exists even for $t_{p3} = t_{p4} = t_{c3} = t_{c4} = 0$. Next, we reduce the half of molecules by introducing the dimerization for the bond between 1(2) and 4(3) sites which are connected by thick arrow in Fig. 1. In terms of such a procedure, Fig. 1 can be replaced by Fig. 7 of anisotropic square lattice consisting of two sites in the unit cell. Thus the model is replaced by the Hamiltonian:

$$H = \begin{pmatrix} 0 & A \\ A^{*s} & 0 \end{pmatrix}$$

$$A = t_{p1} + t_{p2}e^{ik_y} - t_{c1}e^{i(k_x+k_y)} - t_{c2}e^{ik_x} \quad (13)$$

with half-filling. Hereafter we set $t_{p1} = t_{p2} (= 1)$ for the simplicity. Two bands degenerate at \mathbf{k}^0 when off-diagonal component of Eq. (13) equals to zero. The momentum, at which the degeneracy occurs, can be obtained analytically

ically as

$$k_x^0 = \mp 2 \tan^{-1} \left(\sqrt{\frac{2 - t_{c1} - t_{c2}}{2 + t_{c1} + t_{c2}}} \right),$$

$$k_y^0 = \pm 2 \tan^{-1} \left(\frac{\sqrt{(2 - t_{c1} - t_{c2})(2 + t_{c1} + t_{c2})}}{t_{c1} - t_{c2}} \right). \quad (14)$$

Equation(13) gives the symmetric linear dispersion of the Dirac cone with $v^+(\delta\mathbf{k}) = -v^-(\delta\mathbf{k})$, which is different from eq.(7).

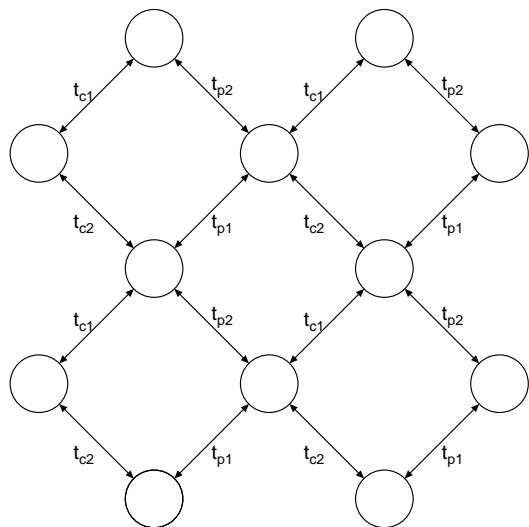


Fig. 7. A model with anisotropic square lattice obtained from Fig. 1 where there are two sites in unit cell.

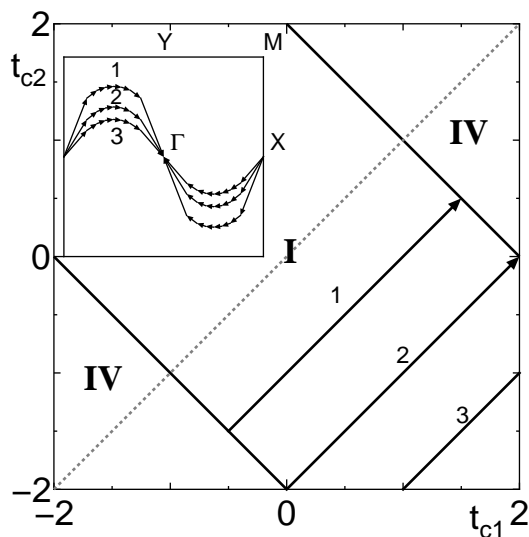


Fig. 8. Phase diagram on the t_{c1} - t_{c2} plane for the model of Fig. 7. Region I is the the same as Figures 6 while region IV corresponds to the insulating state. The inset denotes the trajectory of contact points corresponding to the arrow in the main figure.

Figure 8 shows the t_{c1} - t_{c2} phase diagram based on the model of Fig. 7 where the ZGS state is obtained in the

region I and the insulating state is obtained in the region IV, respectively. The inset shows the positions of contact points on the k_x - k_y plane obtained from Eq. (14) when parameters t_{c1} - t_{c2} are varied as ($C_t = -1, -2, -3$)

$$t_{c2} = t_{c1} + C_t. \quad (15)$$

The corresponding parameters are also shown by the arrow of lines 1, 2 and 3 in the main figure. The boundary between I and III is given by

$$t_{c2} = -t_{c1} \pm 2, \quad (16)$$

respectively. Properties of contact point are as follows. The contact point is located at X for $t_{c2} = -t_{c1} - 2$, and at Γ for $t_{c2} = -t_{c1} - 2$. For $t_{c1} \simeq t_{c2}$, contact points exist near the zone boundary of the k_x - k_y plane. For $t_{c1} = t_{c2}$, two bands degenerate on the zone boundary where $t_{c1} = t_{c2} = 1$ corresponds to the isotropic square lattice. Two bands degenerate at the point and contact point appears when $t_{c1} \neq t_{c2}$, i.e. the symmetry of the bond is broken.

It is found that the ZGS is mainly obtained for $t_{c1}t_{c2} < 0$ although the finite value of other transfer energies are needed for the semimetallic state.

6. Discussion

In the present study, we examined the ZGS state by changing transfer energies within tight-binding model. For α -(ET) $_2$ I $_3$, the hole and electron bands degenerate at two contact points \mathbf{k}^0 and $-\mathbf{k}^0$ in the First Brillouin zone. The dispersions of the electron and hole bands around the contact points resemble that of massless Dirac Fermion, which is called as the Dirac corn. In the wide range of pressures (also transfer energies), there exists the ZGS state, in which the contact point coincides with the Fermi surface. The locations for the contact points move in the momentum space continuously when transfer energies are varied. The stability of the contact point was examined by using the reduced model. The accidental degeneracy disappears when the contact point moves to the symmetry axis or the symmetry point. Such a fact was also verified by using the simplified model.

Those contact points obtained in the present study are relevant to the "accidental degeneracy" of the bands pointed by Herring.¹⁸ In the case of "accidental degeneracy", the degeneracy is not caused by the symmetry of the materials but is caused by the intrinsic properties of the special band. As for the general case of the three-dimensional system, there appear contact lines in the Brillouin zone, which lead to a metal due to the existence of the Fermi surface. The ZGS state of α -(ET) $_2$ I $_3$ exhibits the contact point which always coincides with the Fermi energy, due to the quarter-filled band in the highly two-dimensional system. The existence of such a degeneracy in α -(ET) $_2$ I $_3$ has been supported recently by the first-principle calculation.²⁰

Anomalous properties associated with the Dirac corn, have been investigated for bismuth^{21,22} and graphite²³ by using the effective Hamiltonian for the Dirac corn, while the degeneracy occurs on the symmetry axis of its Brillouin zone. The Berry's phase effect on the Dirac corn

has been observed by using the phase analysis of quantum oscillations.²⁴ Thus the ZGS state of α -(ET)₂I₃ is also expected to exhibit anomalous properties. The new phenomenon known as the anomalous transport^{5, 6, 25} may come from the Dirac cone and the unique properties of the ZGS state

Acknowledgements

The authors are thankful to R. Kondo, S. Kagoshima, T. Takahashi and D. Hirashima for useful comments. The authors are also grateful to S. Sugawara, N. Tajima, Y. Nishio and K. Kajita for useful discussions. The present work has been financially supported by a Grant-in-Aid for Scientific Research on Priority Areas of Molecular Conductors (No. 15073103) from the Ministry of Education, Culture, Sports, Science and Technology, Japan.

- 1) T. Ishiguro, K. Yamaji and G. Saito: *Organic Superconductors* (Springer-Verlag, Berlin, 1998) 2nd ed.
- 2) H. Seo, C. Hotta and H. Fukuyama: *Chem. Rev.* **104** (2004) 5005.
- 3) K. Bender, I. Hennig, D. Schweitzer, K. Dietz, H. Endres and H. J. Keller: *Mol. Cryst. Liq. Cryst.* **107** (1992) 23.
- 4) B. Rothaemel, L. Forro, J. R. Cooper, J. S. Schilling, M. Weger, P. Bele, H. Brunner, D. Schweitzer and H. J. Keller: *Phys. Rev. B* **34** (1986) 704.
- 5) K. Kajita, T. Ojio, H. Fujii, Y. Nishio, H. Kobayashi, A. Kobayashi and R. Kato, *J. Phys. Soc. Jpn.* **61** (1992) 23.
- 6) N. Tajima, M. Tamura, Y. Nishio, K. Kajita and Y. Iye: *J. Phys. Soc. Jpn.* **69** (2000) 543.
- 7) Y. Takano, K. Hiraki, H. M. Yamamoto, T. Nakamura and T. Takahashi: *J. Phys. Chem. Solids* **62** (2001) 393.
- 8) R. Wojciechowski, K. Yamamoto, K. Yakushi, M. Inokuchi and A. Kawamoto: *Phys. Rev. B* **67** (2003) 224105.
- 9) T. Takahashi: *Synth. Met.* **133-134** (2003) 261.
- 10) M. Maesato, Y. Kaga, R. Kondo and S. Kagoshima: *Rev. Sci. Instrum.* **71** (2000) 176.
- 11) N. Tajima, A. Ebina-Tajima, M. Tamura, Y. Nishio and K. Kajita: *J. Phys. Soc. Jpn.* **71** (2002) 1832.
- 12) H. Kino and H. Fukuyama: *J. Phys. Soc. Jpn.* **64** (1995) 4523-4526; *ibid.* **65** (1996) 2158-2169.
- 13) H. Seo: *J. Phys. Soc. Jpn.* **69** (2000) 805.
- 14) A. Kobayashi, S. Katayama, K. Noguchi and Y. Suzumura: *J. Phys. Soc. Jpn.* **73** (2004) 3135.
- 15) A. Kobayashi, S. Katayama and Y. Suzumura: *J. Phys. Soc. Jpn.* **74** (2005) 2897.
- 16) T. Mori, H. Mori and S. Tanaka *Bull. Chem. Soc. Jpn.* **72** (1999) 179.
- 17) R. Kondo and S. Kagoshima: *J. Phys. IV France* **114** (2004) 523 and private communication on the transfer integrals of α -(ET)₂I₃ at $P_a = 2$ kbar and $P_b = 3$ kbar.
- 18) C. Herring, *Phys. Rev.* **52** (1937) 365.
- 19) Another simplified model has been discussed. [S. Sugawara: Master Thesis, Toho University, Chiba (2005); S. Sugawara, N. Tajima, Y. Nishio and K. Kajita: private communication.
- 20) H. Kino, T. Miyazaki and S. Ishibashi, in preparation.
- 21) H. Kohno, H. Yoshioka and H. Fukuyama, *J. Phys. Soc. Jpn.* **61** (1992) 3462.
- 22) P. A. Wolff, *J. Phys. Chem. Solids* **25** (1964) 1057.
- 23) A. A. Abrikosov, *Phys. Rev. B* **60** (1999) 4231.
- 24) I. A. Luk'yanchuk and Y. Kopelevich, *Phys. Rev. Lett.* **93** (2004) 166402.
- 25) K. Kajita, N. Tajima, A. Ebina-Tajima, and Y. Nishio, *Synth. Metal* **133** (2003) 95.